The Interaction of Vapor-Deposited Al Atoms with CO_2H Groups at the Surface of a Self-Assembled Alkanethiolate Monolayer on Gold†

G. L. Fisher,‡ A. E. Hooper,‡ R. L. Opila,§ D. L. Allara,*,‡ and N. Winograd*,‡

Department of Chemistry, The Pennsylvania State University, University Park, Pennsylvania 16802, and Lucent Technologies/AT&T Bell Laboratories, 600 Mountain Avenue, Murray Hill, New Jersey 07974

Received: September 20, 1999; In Final Form: January 4, 2000

The interaction of vapor-deposited Al atoms with self-assembled monolayers of $HS(CH_2)_{15}CO_2H$ chemisorbed at polycrystalline Au(111) surfaces has been studied using time-of-flight secondary-ion mass spectrometry, X-ray photoelectron spectroscopy, and infrared spectroscopy. The Al deposition was performed incrementally at room temperature. The Al atoms do not penetrate into the organic monolayer, but rather they remain at the vacuum interface where they undergo chemical interactions solely with the CO_2H groups. Reaction of the CO_2H groups continues until slightly more than one atom per reacting group is deposited, on average; thereafter, no further reaction is observed. However, 20−25% of the CO_2H groups remain unreacted, regardless of the Al coverage. These results are explained on the basis of a combination of chemical and steric effects.

1. Introduction

Extensive studies have been made on metal−organic interfaces by evaporating metals onto organic thin films[1−11] and polymers.[12−24] These studies, while very informative as to the general behavior of metal atoms at organic surfaces, have suffered generally from a lack of quantitative control of the surface density and placement of the specific organic functional groups of interest as well as from insufficient characterization of both the molecular and the metal states of the surface complexes formed.

In recent studies,[25,26] we have approached this problem for the specific case of Al-atom interactions through the use of well-defined substrates prepared by surface self-assembly in conjunction with in situ, multitechnique analyses. In an initial study involving methyl ester- and methyl-terminated alkanethiolate monolayers on gold,[26] we observed that Al atoms react in a ∼1:1 fashion with the ester group, whereas, with the methyl group, no chemical interactions occur. In the ester case, all of the Al atoms remained at the monolayer surface (vacuum interface), whereas, in the methyl case, Al atoms initially penetrate into the alkyl chain matrix and form an adlayer at the Au−S interface region. An interesting aspect of the ester monolayer system is that, after the initial reaction of all of the ester groups, approximately four additional Al atoms continue to form organometallic reaction products, as evidenced by the appearance of Al in positive valence states. Subsequent Al-atom deposition results in the growth of a metallic film. It was concluded that the lack of Al penetration into the ester monolayer is due to the reactivity of the ester groups; thus, these groups act as chemical traps for the impinging Al atoms. Because the efficiency of such a trap is directly dependent on the reactivity of the surface group, it is important to learn which chemical features control this reactivity and for which types of organic groups the penetration channel could be competitive with formation of organometallic products at the surface. With this goal in mind, we decided to examine the behavior toward Al deposition of a series of monolayers formed by chemisorption of $X(CH_2)_nSH$ on Au, where X = OH, OCH_3, and CO_2H. These groups are all related closely to the CO_2CH_3 structure so that a study of the reactivities, relative to the degrees of penetration, would offer a broad picture of the behavior of monolayers terminated by simple oxygen-containing groups.

In the present study, we report about Al-atom deposition on a $HO_2C-(CH_2)_{15}S/Au$ monolayer. The results, based on time-of-flight secondary-ion mass spectrometry (ToF-SIMS), X-ray photoelectron spectroscopy (XPS), and infrared spectroscopy (IRS) analyses, show that the CO_2H group is sufficiently reactive to prevent penetration into the monolayer. However, an important contrast exists between the CO_2CH_3 and CO_2H systems with respect to the average number of Al atoms required to destroy the chemical integrity of the surface groups. In the CO_2CH_3 case, approximately one Al atom destroys the original chemical integrity of each ester group with all ester groups reacting. In the CO_2H case, continued Al deposition never results in more than ∼75−80% of the CO_2H groups reacting, and this reaction is complete with slightly more than one Al atom per reacted group. These results underscore the complexity of the organometallic chemistry that can ensue at an Al−organic interface.

2. Experimental Section

2.1. Sample Preparation. The preparation and characterization of acid-terminated self-assembled monolayers (SAMs) has been described in detail previously.[27] Briefly, the Au substrates were prepared on native-oxide-covered Si(001) wafers having a Cr adhesion layer. The Au surface layer, 2000 Å thick, was evaporated from a resistively heated Al_2O_3-coated W-boat onto a Cr adhesion layer, 100 Å thick, that was evaporated from a resistively heated Cr/W-rod. All metals had purities ≥99.99%. Immersion of the gold films into millimolar solutions of thiol in absolute ethanol for 4 days yielded well-organized monolayer films, as shown by ellipsometry, IRS, and contact angle measurements.[27]

† Part of the special issue "Gabor Somorjai Festschrift".
‡ The Pennsylvania State University.
§ Lucent Technologies/AT&T Bell Laboratories.

10.1021/jp993354p CCC: $19.00
Published on Web 02/29/2000

2.2. ToF-SIMS. The ToF-SIMS analyses were performed on a custom-designed instrument.[28] The instrument consists of a loadlock, a preparation chamber, and the primary analysis chamber, each separated by a gate valve. The primary ions are delivered using a Ga^+ liquid-metal ion gun (LMIG). The primary ion beam is accelerated to 25 keV and has a probe diameter of 100 nm. The secondary ions are focused into a flight tube by an extraction lens, allowed to drift through a field-free region into a two-stage reflectron where they are time compressed, allowed to drift through a second field-free region, and finally allowed to strike the multichannel plate (MCP) detector. During data acquisition, the beam is pulsed with a width of 40 ns at $\leq$2 nA and is rastered over a 1600 $\times$ 1600 μm^2 area. All spectra were acquired using a total ion dose of less than 10^{11} ions/cm^2. Relative peak intensities are reproducible to within $\pm$6% from sample to sample and $\pm$6% from scan to scan.

Room-temperature deposition of Al, using a W-wire basket source, was performed in the preparation chamber at a rate of 0.1 Å/s. Deposition measurements were made using a Sycon STM-100 quartz crystal microbalance (QCM) controller. Maximum error within the deposition measurements is $\pm$8%. The pressure remained below 5 $\times$ 10^{-8} Torr during the Al deposition. The base pressure of the system is 1.5 $\times$ 10^{-9} Torr, which was recovered before sample transfer.

2.3. XPS. The XPS analyses were performed on a Scienta ESCA 3000 spectrometer equipped with a monochromatic Al K_α source and is described in detail elsewhere.[29,30] A pass energy of 75.00 eV and an energy step of 0.05 eV were used for the analysis. The resulting full width at half-maximum (fwhm) for Au $4f_{7/2}$ is 0.52 eV. A binding energy of 84.00 eV for Au $4f_{7/2}$ was used as a reference for all spectra.

Following analysis of the bare monolayer, the sample was transferred under vacuum to the Al evaporation chamber, which is isolated from the analysis chamber by a gate valve. The pressure in the preparation chamber remained below 1 $\times$ 10^{-8} Torr during the deposition. Incremental amounts of Al were deposited at a rate of 1.0 Å/min by evaporation from a graphite crucible heated to 975 K. The deposition rate was checked periodically by removing a reference sample and analyzing it with Rutherford backscattering spectroscopy. The Al/SAM specimen was transferred, without exposure to air, to the analysis chamber.

2.4. IRS. Analyses were performed on a Mattson Research Series instrument with custom optics optimized for grazing incidence reflection. A liquid-nitrogen-cooled mercury−cadmium−telluride (MCT) detector was used with an effective frequency range of ~750−8000 cm^{-1}. The infrared beam was allowed to access the vacuum system and reflect from the sample through a pair of differentially pumped KBr windows. All of the optics and electronics were positioned outside the vacuum system with only the IR beam entering the vacuum chamber. After analysis of the bare monolayer, a shield was opened between the sample and the Al source. The Al was evaporated from a W-wire basket at a rate of 1.0 Å/min, as measured by a QCM. The pressure remained below 1 $\times$ 10^{-7} Torr during the deposition.

3. Results

3.1. Monolayer Coverage. Monolayer coverage is defined as the mass of deposited Al that contains 4.6 Al atoms/nm^2, the average surface density of thiolate molecules at the Au surface. The amount of deposited Al also has been converted to an equivalent thickness, on the basis of the density of bulk aluminum, so that d_{Al} = 0.9 Å = 1.0 monolayer (ML).[26]

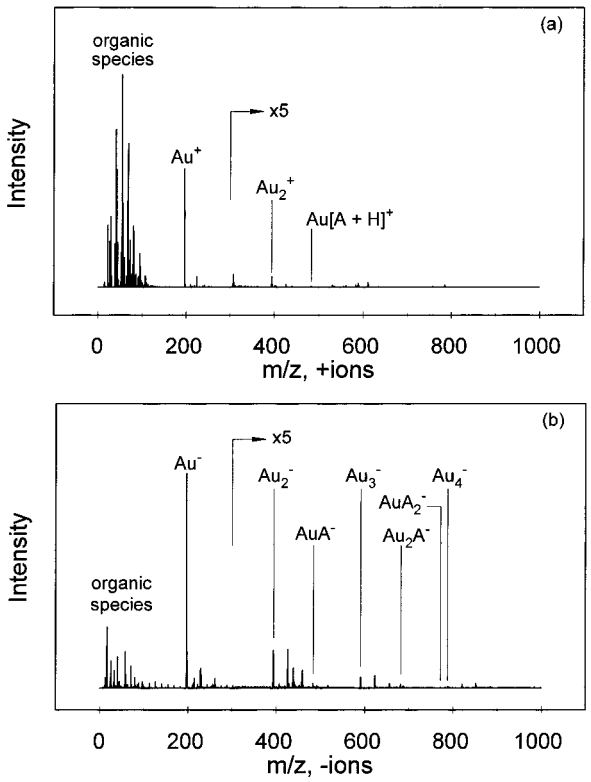

Figure 1. (a) Positive SIMS spectrum showing the 0−1000 *m/z* region of the bare acid-terminated monolayer on Au(111). (b) Negative SIMS spectrum showing the 0−1000 *m/z* region of the same monolayer system. The molecular adsorbate, $S(CH_2)_{15}CO_2H$ (*m/z* 287), is given the symbol A. In both spectra, the region of the spectrum beyond *m/z* = 300 has been multiplied by a factor of 5.

3.2. ToF-SIMS. The ToF-SIMS spectra for both positive and negative ions were collected using the conditions detailed in section 2.2. In general, we find that the relative intensities of the Au_x^-, $Au_xS_y^-$, and SO_x^- ions provide a useful indication that the sample has been prepared without substantial incorporation of impurities or oxidative products.[31,32] These cluster ion intensities are similar to those reported previously for other monolayers.[26,31,33,34]

The information associated with the positive ion spectrum of the bare monolayer, shown in Figure 1a, is found mostly below a mass-to-charge ratio (*m/z*) of 200, with the exception of the Au_x^+ and $Au_xS_y^+$ cluster ions. A weak protonated molecular ion associated with Au is also observed at *m/z* = 485. However, more commonly observed species that are indicative of the adsorbate molecule are those formed by the loss of H_2O and CO_2. Common fragment ion moieties are $(CH_2)_xCH^+$, $S_x(CH_2)_y^+$, and $[AuS(CH_2)_x]H^+$. Other, less prominent, features in the positive ion spectrum have the general forms $[(CH_2)_xCO]^+$ and $[(CH_2)_xCO_2H]H^+$.

The negative ion spectrum of the bare monolayer, shown in Figure 1b, exhibits a number of high-mass peaks containing the intact acid-terminated alkanethiolate, A = $S(CH_2)_{15}CO_2H$, as well as a number of important fragment ions. Mass peaks involving intact adsorbate species are AuA^- at *m/z* = 484, Au_2A^- at *m/z* = 681, and AuA_2^- at *m/z* = 771. Other ions of interest are $(CH_2)_xCO_2^-$, $[(CH_2)_xCO]H^-$, $(CH_2)_xS_y^-$, and $[AuS(CH_2)_x]^-$. Negative ions in the mass range of 580−820 are shown in Figure 2a.

Following analysis of the bare monolayer, Al is deposited incrementally, and analyses are performed at average Al thicknesses (d_{Al}) of 0.5, 1.0, 2.0, and 4.0 Å. Changes in intensity are tracked for the aforementioned fragments, as well as for

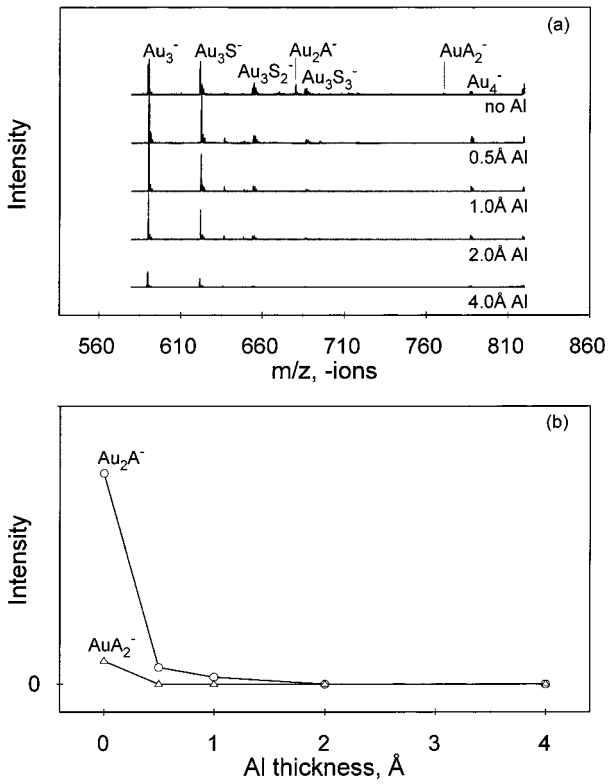

Figure 2. (a) Negative SIMS spectra showing the 580−820 *m/z* region of the acid-terminated monolayer prior to and following deposition of Al. (b) Integrated peak area of Au_2A^- and AuA_2^- plotted versus d_{Al}.

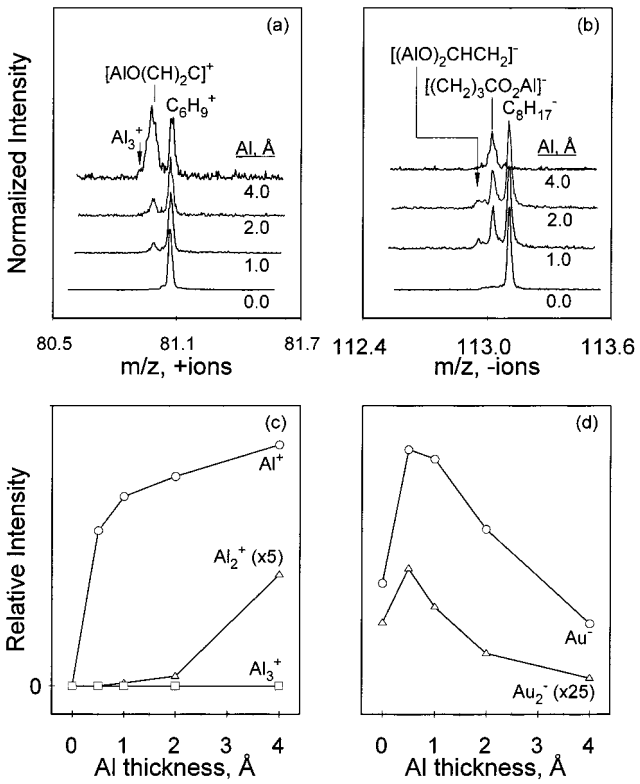

Figure 3. High-resolution spectral overlays following progression of metal−organic fragments with Al deposition. (a) Positive ions, nominal mass 81 amu. (b) Negative ions, nominal mass 113 amu. The spectra are normalized to the initial peak intensities of $C_6H_9^+$ and $C_8H_{17}^-$, respectively. (c) Integrated peak areas of Al^+, Al_2^+, and Al_3^+ plotted versus d_{Al}. (d) Integrated peak areas of Au^- and Au_2^- plotted versus d_{Al}.

new features in the mass spectrum. The rapid disappearance of oxygen-containing fragments from the mass spectra is a prominent feature of Figure 2a. Hydrocarbon peak intensities remain relatively unchanged during early stages of the deposition, as do the intensities of metal clusters from the Au substrate. As the deposition progresses, though, the intensities of all of the peaks, except for the Al_x^+ peaks, become attenuated by thickening Al overlayers.

The areas of the peaks involving intact adsorbate molecules, specifically Au_2A^- and AuA_2^-, are plotted versus d_{Al} in Figure 2b. From these data, it is possible to discern qualitative information about the number of Al atoms that are attached to each organic functional group. These curves are similar to those reported for Al depositions on the methyl ester-terminated SAM reported in Figure 8 of ref 26. For both of these plots, the AuA_2^- peaks after deposition of 1 Å of Al nearly vanishes, although there is still significant Au_2A^- intensity observed for the acid-terminated SAM. Because there was shown to be one Al atom per ester group, these results suggest that there is slightly more than one Al atom associated with each initially reacting functional group.

The observable trends of Figure 2 are further detailed in Figure 3a,b. Here, isobaric peaks at nominal masses of 81 and 113 amu, respectively, are plotted versus d_{Al}, showing the formation of unidentate and bidentate species. The spectra are normalized to the initial peak intensities of $C_6H_9^+$ and $C_8H_{17}^-$ to make obvious the increasing intensity of the metal−organic fragments with respect to the hydrocarbon fragments as the deposition progresses. On the basis of a recording of the area under these peaks, it is possible to show that the metal−organic fragments achieve their highest intensity at $d_{Al} \sim 2.0$ Å and then decrease in intensity as the overlayer becomes covered with Al atoms. The chemical interaction between deposited Al and the terminal functional group is evident through observation of fragments such as $[AlO(CH)_2C]^+$ and $[(CH_2)_3CO_2Al]^-$. The presence of the $[(AlO)_2CHCH_2]^-$ fragment ion shown in Figure 3b is another piece of evidence indicating that more than one Al atom is chemisorbed per organic functional group.

Other observed metal−organic species indicative of the interface structure are AlO^-, $AlOC^+$, $AlOC(CH_2)_x^{\pm}$, $AlO_2C(CH_2)_x^{\pm}$, $Al_2O_2C(CH_2)_x^{\pm}$, and $[S_x(CH_2)_{15}CH(OH)(OAl)]^{\pm}$. Of special note is the $CH(OH)(OAl)^+$ fragment ion. Such species appear with the first increment of deposited Al and remain throughout the deposition regime. The persistence of these peaks suggests that some residual functional group oxygen atoms, particularly those in the hydroxyl form, remain unreacted with deposited Al.

Ions of the forms $Au_xAl_yS_z^-$, AlS_x^-, and $AlS(CH_2)_x^+$, which indicate penetration of Al to the monolayer−Au interface, are not observed in the spectra. Other peaks that are not observed in the mass spectra with any significant intensity are AlO_2^- and $Al_2O_3^-$. These data, when compared to the results of previous studies,[20,21,23−26] clearly suggest that the Al atoms interact directly with the oxygen of the acid-terminated monolayer, without removing the oxygen atoms from the functional group, to form discrete metal−organic complexes. Moreover, deposited Al does not significantly penetrate to the monolayer−Au interface. The ToF-SIMS data consistently indicate that the metal−organic bonds have an Al−O−C structure.

The extent to which deposited Al penetrates through the monolayer to the monolayer−Au interface or forms an overlayer can be extracted, in part, from a plot of the Al^+, Al_2^+, and Al_3^+ intensities versus d_{Al}, as shown in Figure 3c. We have shown previously that these signal intensities differ between the case in which deposited Al is known to penetrate through the

monolayer to the monolayer−Au interface (methoxy- and methyl-terminated) and the case in which deposited Al chemisorbs at the monolayer−vacuum interface where it forms a dielectric (methyl ester- and hydroxyl-terminated).[25,26]

When Al is deposited onto the methyl ester- and hydroxyl-terminated monolayers, only Al^+ is observed below the saturation limit (1:1 ratio of deposited Al to reactive oxygen). Appreciable levels of Al_2^+ and Al_3^+ are observed only after the functional groups have reacted, before which the overlayer consists primarily of isolated Al atoms bound to organic functional group oxygens (those capable of chemisorption). The appearance of peaks from Al_n^+ clusters in the spectra indicates that the Al is depositing as clusters.[35] Thus, a stoichiometry of one Al atom per functional group was observed in both cases. Note that, in the case of the methyl ester termination, the ether linkage is not involved in chemisorption, at least not to the point at which any of the C−O−C bonds are broken.[26]

The trend in the Al_x^+ cluster data for Al deposited onto an acid-terminated monolayer is similar to those reported for Al deposited onto the methyl ester- and hydroxyl-terminated monolayers. As shown in Figure 3c, the Al^+ signal dominates at $d_{Al} < 1.5$ Å, and appreciable levels of Al_2^+ appear only after $d_{Al} > 2.0$ Å. No Al_3^+ signal is observed in this deposition regime (also see Figure 3a). These data indicate that, at low coverages, the overlayer consists primarily of isolated Al atoms bound to acid functional groups. Furthermore, the appearance of Al_2^+ in the mass spectrum does not occur until $d_{Al} \geq 2.0$ Å, and Al_3^+ is not observed at all. We conclude from these data that two Al atoms are bound per acid functional group (or one Al atom per oxygen). Indeed, the stoichiometry of Al to acid functional groups, as indicated by the Al_x^+ cluster data, is in agreement with that of Figure 2b ($Au_xA_y^-$ vs d_{Al}).

Additional information concerning Al penetration and overlayer formation can be inferred from the Au^- and Au_2^- intensities plotted versus d_{Al}, as shown in Figure 3d. With the first increment of deposited Al, these ion yields increase as a result of electron transfer from the relatively electropositive Al atoms at the vacuum interface to the relatively electronegative Au atoms and clusters leaving the surface.[36] However, upon subsequent depositions of Al, these signals are quickly attenuated by the metal−organic interface and metallic overlayers, which block ejection channels. This trend is similar to that reported for Al deposited onto methyl ester- and hydroxyl-terminated monolayers for which the metal−organic interaction is strong.[25,26] We therefore conclude, on the basis of the Al_x^+ and Au_x^- cluster data, that the deposition of Al atoms onto an acid-terminated monolayer leads to the formation of a chemisorbed metal−organic layer followed by the formation of metallic overlayers.

3.3. XPS. The C 1s, O 1s, and Al 2p core-level shifts of the acid-terminated monolayer prior to and following deposition of Al are shown in Figure 4. The data were collected at a 10° takeoff angle, which improved the signal-to-noise ratio and slightly enhanced surface selectivity. The spectra were all shifted so that the Au $4f_{7/2}$ energy was exactly 84.00 eV. The core-level spectra of this monolayer reveal two types of carbon atoms, at binding energies of 285.50 and 289.45 eV, which correspond to CH_2 and COO, respectively (Figure 4a). A single O 1s peak at 532.75 eV is assigned to the COO oxygen atoms (Figure 4b). We do not observe any resolution of separate peaks from the C═O and the C−OH oxygens. The extensive hydrogen bonding between adjacent CO_2H groups (see IRS data in the next section) would serve to redistribute the electron density on these atoms and move their binding energies closer than the corresponding energies for isolated groups. These C and O binding-energy assignments agree with those reported for poly(acrylic acid) films[20] within the resolution of the measurements.

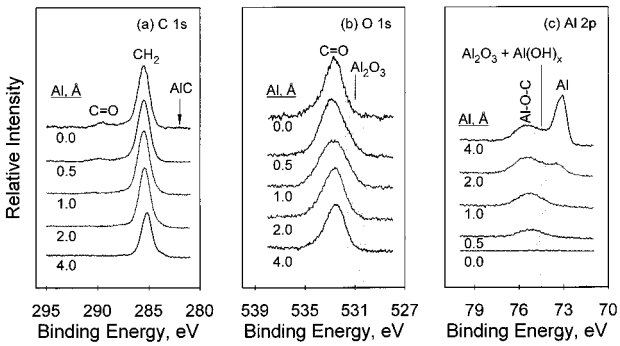

Figure 4. Core-level XPS spectra of the acid-terminated monolayer prior to and following deposition of Al. (a) The C 1s core-level spectra. (b) The O 1s core-level spectra. (c) The Al 2p core-level spectra.

The chemical shifts are noticeably altered upon deposition of Al. The carboxyl C 1s peak in Figure 4a has shifted to higher binding energy (289.90 eV) and has decreased in intensity by $d_{Al} = 0.5$ Å. This change is followed by complete loss of the carboxyl C 1s peak by $d_{Al} \leq 2.0$ Å; however, the signal approaches the baseline when $d_{Al} \sim 1.0$ Å. The methylene C 1s peak shifts to lower binding energy (285.15 eV), and a slight decrease in signal is realized early in the deposition. This shift to lower binding energy is indicative of a higher electron density on the carbon at the tail end of the monolayer. A peak associated with the formation of AlC, expected at 282.30 eV, is not observed.

Examination of Figure 4b shows that the O 1s peak is broadened with the first increment of deposited Al and is centered at a slightly higher binding energy of 532.90 eV. The observed peak broadening suggests the presence of two oxygen species that are close in energy. When $d_{Al} > 1.0$ Å, the O 1s peak becomes sharper and becomes centered at 532.50 eV. These observations imply that the oxygen atoms, upon reaction with deposited Al, occupy the same chemical state as, but are compositionally different from, the oxygen atoms of the bare monolayer. The loss of the carboxyl C 1s peak, mentioned above, together with the O 1s core-level data suggests that both oxygen atoms of the acid functional groups react with deposited Al to form metal−organic complexes.

Analysis of the Al 2p spectra in Figure 4c reveals the appearance of a peak centered at 75.50 eV when $d_{Al} \sim 0.5$ Å. This peak is shifted ~1 eV higher than expected for Al_2S_3 and ~1.5−2.0 eV higher than expected for the Al_2O_3 and $Al(OH)_x$ species. We assign this peak to the formation of a metal−organic species upon chemisorption of deposited Al at the acid group. When $d_{Al} > 4.0$ Å, another peak appears at 72.90 eV, corresponding to metallic Al. An intermediate phase exists between chemisorption of the initially deposited Al ($d_{Al} \leq 0.5$ Å) and formation of a metallic overlayer ($d_{Al} > 4.0$ Å). This phase is electron-deficient relative to the metallic phase, as evidenced by the appearance of an Al 2p peak at 73.50 eV, which is 0.60 eV higher in binding energy than the metallic Al peak.[23−26] In total, these data indicate that, as the deposition progresses, Al atoms bind with both oxygen atoms of the acid functional group to form metal−organic species. This stage is followed by the formation of a premetallic region and then metallic overlayers.[20,21]

3.4. IRS. The spectra of the acid-terminated monolayer, before and after deposition of Al, are shown in Figure 5. The peak assignments of the bare monolayer have been reported

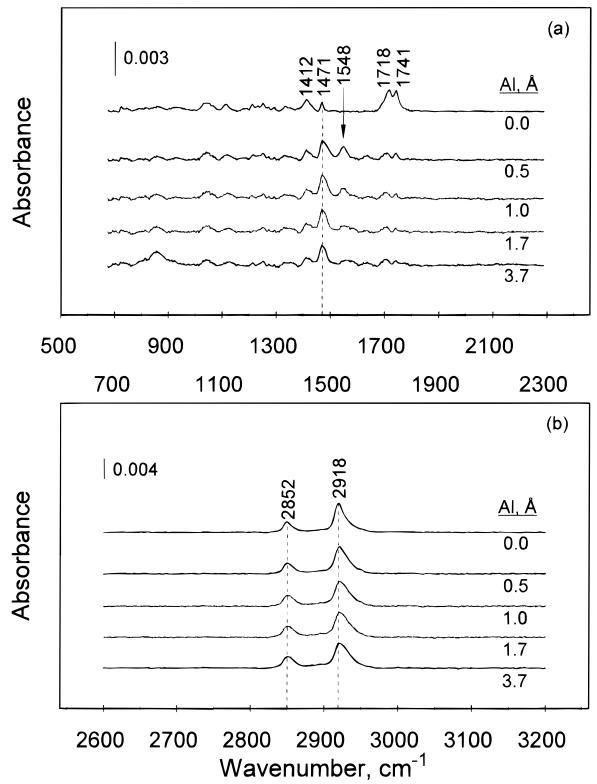

Figure 5. Infrared reflectance spectra of the acid-terminated monolayer prior to and following deposition of Al. (a) Low-frequency region, 700−2300 cm^{-1}. (b) High-frequency region, 2600−3200 cm^{-1}. Dashed lines are used to highlight several important spectral features.

previously[41] and are outlined here for ease of comparison. The absorption bands at 1412 and 1471 cm^{-1} are assigned as the CH_2 (α- and main-chain, respectively) scissor deformation modes (γ_{CH_2}) of alkyl chains. The bands at 1718 and 1741 cm^{-1} correspond to hydrogen-bonded and non-hydrogen-bonded carbonyl stretches ($\nu_{C=O}$), respectively. Finally, the C−H symmetric (d^+) and antisymmetric (d^-) stretches are assigned at 2852 and 2918 cm^{-1}, respectively. These data indicate that the chains in the starting monolayer are well-ordered conformationally and fully extended.[27]

The low-frequency region of the spectra, shown in Figure 5a, indicates that features related to the functional group are significantly perturbed upon deposition of Al. For increasing Al coverages up to $d_{Al} \sim 1$ Å, the intensities of the carbonyl absorption bands at 1718 and 1741 cm^{-1} decrease equally until ∼20−25% of the CO_2H groups remain unreacted (as determined by peak areas). These trends are shown in Figure 6. A simple analysis of these data suggests that 1.1 Al atoms are consumed per reacted functional group. In addition, the H-bonded carbonyl band at 1718 cm^{-1} shifts 14 cm^{-1} toward lower frequency. For $d_{Al} > 1$ Å, the residual carbonyl signal remains constant, indicating no further reaction. This measurement is discussed more fully in section 4.

Except for a slight drop in intensity, the α-CH_2 scissors absorption at 1412 cm^{-1} remains unchanged at all Al coverages. However, the main-chain CH_2 scissor deformation at 1471 cm^{-1} becomes broader and more intense. Conformational disordering of the chains is indicated by these observations and presumably arises from distortions of the CO_2H group positions at the monolayer surface caused by reactions with Al atoms.

There are two new features in the low-frequency region of the spectra that arise upon Al deposition. The first, centered at 1548 cm^{-1}, appears immediately and decreases in intensity to a limiting value as the deposition progresses. This feature appears in a region typical for the antisymmetric C−O stretch of a carboxylate (CO_2) group. The failure of this absorption to completely vanish indicates that portions of the monolayer surface become isolated or screened from further reaction with Al atoms. The second feature is an Al−O stretch, centered at 855 cm^{-1}, that appears when $d_{Al} \geq 2.0$ Å. This absorption, in the general region of the Al−O vibrations of Al_2O_3,[37] clearly indicates the formation of Al−O bonds.

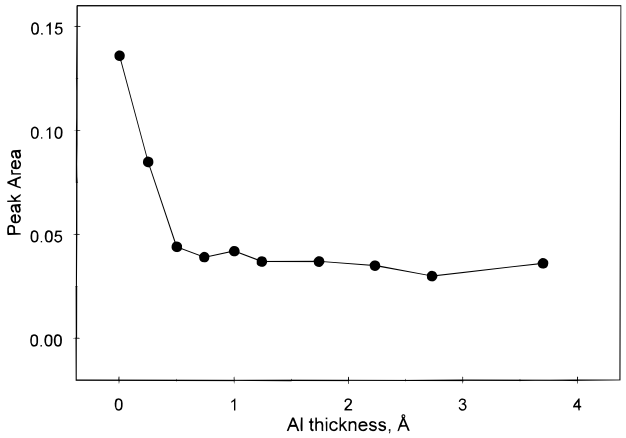

Figure 6. Plot displaying the combined integrated peak area of the $\nu_{C=O}$ modes versus d_{Al}.

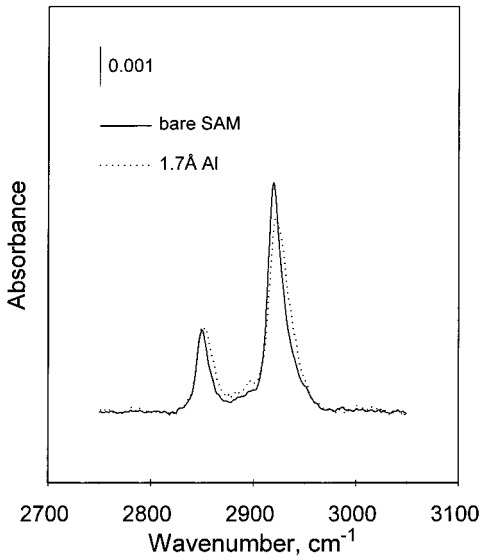

Figure 7. Overlay of the infrared reflectance spectra of the bare acid-terminated monolayer and the same region of the spectrum after 1.7 Å of Al has been deposited.

The high-frequency region of the spectrum, shown in Figure 5b, indicates that the d^+ and d^- mode peaks shift to higher frequency, 2 and 3 cm^{-1}, respectively, and broaden for $d_{Al} \sim 1.0$ Å. These results indicate some degree of conformational disordering of the alkyl chains, consistent with the observed perturbations of the γ_{CH_2} mode (see above). The spectral perturbations are readily seen by overlaying the spectrum from the 1.7-Å deposition and the spectrum from the bare acid-terminated monolayer, shown in Figure 7.

In other studies of monolayers with terminal OH groups,[38] we have observed an Al−H stretch, centered at 1915 cm^{-1} (fwhm = 125 cm^{-1}).[39,40] The absence of a similar absorption band in the current study may indicate a subtle shift so that Al−H bonds in Al−carboxylate species are less stable than in

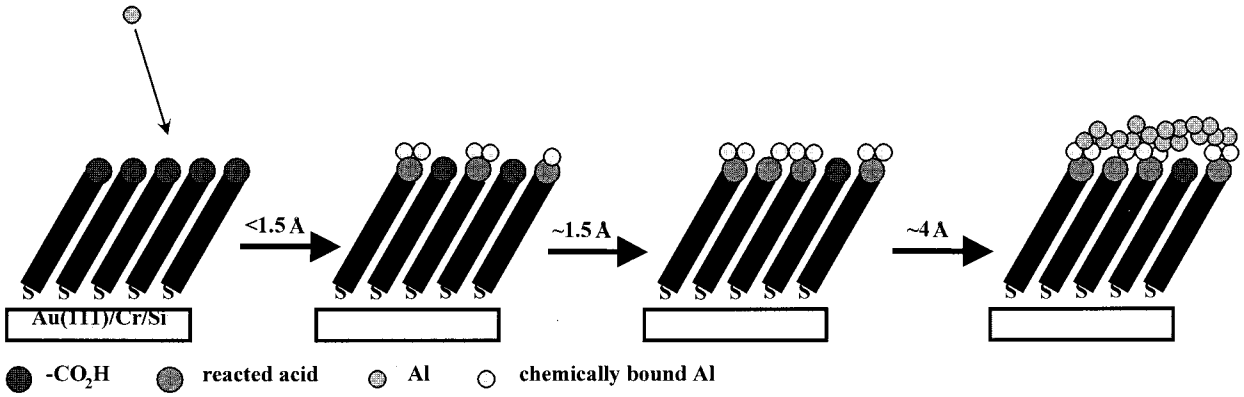

Figure 8. Cartoon illustration of the important features and interaction regimes of deposited Al with an acid-terminated organic monolayer. These structures are based on the combined ToF-SIMS, XPS, and IR data.

Al−alkoxy species. Alternatively, the Al−H bonds may form but may be oriented parallel to the surface, thereby diminishing the IR intensity.

4. Discussion

From previous studies it is clear that vapor-deposited Al atoms react with the carbonyl group of a terminal methyl ester group but are unreactive with CH_2 groups.[26] In this work, we conclude that the CO_2H groups are the sole reaction center. The main findings of the present study are that reaction ceases after between one and two Al atoms are deposited per functional group and that ~20−25% of the CO_2H groups remain unreacted, regardless of coverage. Given the immediate reaction of the CO_2H groups at low coverages, the existence of a residual fraction of unreactive CO_2H groups at high Al coverages indicates subtle steric and/or mechanistic phenomena. One possibility is that the growing Al film assumes a morphology in which steric barriers arise that protect or screen isolated CO_2H-group domains at the surface. Because the IR data shown in Figure 5 reveal that a fraction of the CO_2H groups always remain H-bonded, the isolated domains of groups must consist of at least several groups that can self-interact.

A second possibility is that Al is preferentially reactive with CO_2H groups that are in the H-bonded state. Disruption of hydrogen bonding upon initial deposition of Al at a specific H-bonded group may increase the activation barrier to alkoxy−Al insertion at the neighbor group, with the result that subsequent Al atoms nucleate at existing metal−organic complexes. Given the signal-to-noise characteristics of the C=O stretching mode spectra (Figure 5), one cannot quantitatively assess the exact fractions of reacted types of CO_2H groups.

There are several reaction product structures to consider as possibly underlying the observed ToF-SIMS, XPS, and IRS data, as shown below.

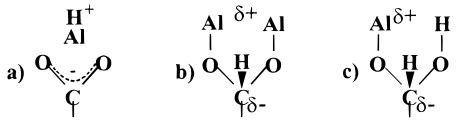

In the mass spectra, there are several $AlO_2C(CH_2)_x^{\pm}$ fragments that appear following deposition of Al. The XPS spectra support a symmetrical structure with equivalent O atoms, because a single O 1s peak is observed following Al deposition. The IRS data indicate the existence of a carboxylate anion, as supported by the absorption band at 1548 cm^{-1}, following Al deposition. Moreover, the IRS data reveal no evidence for the presence of an Al−H stretch or for the presence of an Al−O absorption. However, structure **a** seems a likely candidate for the major reaction product.

Structure **b** may exist as a minor product, as suggested by the observation of $[(CH_2)_xCH(OH)(OAl)]^{\pm}$ cluster ions in the ToF-SIMS spectra. This species is not supported by the XPS or the IRS data, however, and is considered an unlikely product.

Because both the ToF-SIMS and the IRS data suggest that it is possible for more than one Al atom to be present on each reacted functional group, small amounts of a moiety similar to structure **c** may be formed. The ToF-SIMS spectra reveal a $Al_2O_2(CH_2)_x^{\pm}$ cluster ion, although the intensity of its signal is quite low. Moreover, the Al−O vibrational strectching mode at 855 cm^{-1} is weaker than the Al−O stretches found in other ω-functionalized monolayer systems.[25,26,28] Hence, this structure may only occur in small concentrations. This sort of species involves the bonding of Al atoms at oxygen sites via bridged intermediates[41] and alkoxy−Al insertion mechanisms.[42−47]

Once CO_2H−Al reaction ceases at $d_{Al} \sim 1.5$ Å, further deposition of Al results in the formation of positive-valence Al species, as evidenced by the appearance of a high-binding-energy Al 2p peak in the XPS data[20,21] and the appearance of Al_2^+ in the mass spectra.[25,26] Finally, metallic overlayers form when $d_{Al} > 4.0$ Å, as supported by the XPS data.[20,21] A schematic diagram of the deposition process, as deduced from the experimental data, is shown in Figure 8.

5. Conclusions

The body of data presented here indicate that Al reacts readily, although not to completion, with terminal CO_2H functional groups in self-assembled alkanethiolate monolayers on Au. The data indicate that between one and two Al atoms are chemisorbed per acid functional group. The existence of isolated, unreactive CO_2H domains could be due to steric and/or chemical factors. Following chemisorption of the first monolayer of deposited Al, the next 2−4 ML of deposited Al form Al organometallic products, while further deposition results in metallic overlayers. Bonding at the metal−organic interface appears to consist of a mix of ($Al-H^+$ cation)−(CO_2^- anion) complexes and σ-bonded Al−O−C linkages. Finally, consistent with previous studies with the methyl ester group, we find that Al neither reacts with the methylene backbone of the monolayer to form carbides nor significantly penetrates through the monolayer to the monolayer−Au interface.

Acknowledgment. The authors wish to acknowledge the assistance of A. C. Miller in obtaining the XPS data. Financial

support for this research was provided by the Office of Naval Research and the National Science Foundation.

References and Notes

(1) Jung, D. R.; Czanderna, A. W. *Crit. Rev. Solid State Mater. Sci.* **1994**, *19*, 1.
(2) Jung, D. R.; Czanderna, A. W.; Herdt, G. C. *J. Vac. Sci. Technol.* **1996**, *A14*, 1779.
(3) Czanderna, A. W.; King, D. E.; Spaulding, D. *J. Vac. Sci. Technol.* **1991**, *A9*, 2607.
(4) Jung, D. R.; King, D. E.; Czanderna, A. W. *J. Vac. Sci. Technol.* **1993**, *A11*, 2382.
(5) Konstadinidis, K.; Zhang, P.; Opila, R. L.; Allara, D. L. *Surf. Sci.* **1995**, *338*, 300.
(6) Tarlov, M. J. *Langmuir* **1992**, *8*, 80.
(7) Dressick, W. J.; Dulcey, C. S.; Georger, J. H., Jr.; Calabrese, G. S.; Calvert, J. M. *J. Electrochem. Soc.* **1994**, *141*, 210.
(8) Jung, D. R.; King, D. E.; Czanderna, A. W. *Appl. Surf. Sci.* **1993**, *70/71*, 127.
(9) Herdt, G. C.; Czanderna, A. W. *Surf. Sci. Lett.* **1993**, *297*, L109.
(10) Hirose, Y.; Kahn, A.; Aristov, V.; Soukiassian, P. *Appl. Phys. Lett.* **1996**, *68*, 217.
(11) Herdt, G. C.; King, D. E.; Czanderna, A. W. *Z. Phys. Chem.* **1997**, *202*, 163.
(12) Mittal, K., Lee, K.-W., Eds. *Polymer Surfaces and Interfaces: Characterization, Modification and Applications*; VSP International Science Publishers: Zeist, The Netherlands, 1997; pp 189−224.
(13) Atanasoska, Lj.; Anderson, S. G.; Meyer, H. M., III; Zhangda, L.; Weaver, J. H. *J. Vac. Sci. Technol.* **1987**, *A5*, 3325.
(14) Bartha, J. W.; Hahn, P. O.; LeGoues, F.; Ho, P. S. *J. Vac. Sci. Technol.* **1985**, *A3*, 1390.
(15) Ho, P. S.; Hahn, P. O.; Bartha, J. W.; Rubloff, G. W.; LeGoues, F. K. *J. Vac. Sci. Technol.* **1985**, *A3*, 739.
(16) Pireaux, J. J.; Vermeersch, M.; Gregoire, C.; Thiry, P. A.; Caudano, R. *J. Chem. Phys.* **1988**, *88*, 3353.
(17) Vasile, M. J.; Bachman, B. J. *J. Vac. Sci. Technol.* **1989**, *A7*, 2992.
(18) Domingue, A.; Dignard-Bailey, L.; Sacher, E.; Yelon, A.; Ellis, T. H. *ACS Symp. Ser.* **1990**, *440*, 272.
(19) Selmani, A. *ACS Symp. Ser.* **1990**, *440*, 345.
(20) Dekoven, B. M.; Hagans, P. L. *Appl. Surf. Sci.* **1986**, *27*, 199.
(21) Bou, M.; Martin, J. M.; Le Mogne, Th. *Appl. Surf. Sci.* **1991**, *47*, 149.
(22) Lazzaroni, R.; Bredas, J. L.; Dannetun, P.; Logdlund, M.; Uvdal, K.; Salaneck, W. R. *Synth. Met.* **1991**, *41*−*43*, 3323.
(23) Akhter, S.; Zhou, X.-L.; White, J. M. *Appl. Surf. Sci.* **1989**, *37*, 201.
(24) Stoyanov, P.; Akhter, S.; White, J. M. *Surf. Interface Anal.* **1990**, *15*, 509.
(25) Fisher, G. L.; Hooper, A. E.; Opila, R. L.; Jung, D. R.; Allara, D. L.; Winograd, N. *J. Electron Spectrosc. Relat. Phenom.* **1998**, *98*−*99*, 139.
(26) Hooper, A. E.; Fisher, G. L.; Konstadinidis, K.; Jung, D. R.; Nguyen, H.; Opila, R. L.; Collins, R. W.; Winograd, N.; Allara, D. L. *J. Am. Chem. Soc.* **1999**, *121*, 8052.
(27) Nuzzo, R. G.; Dubois, L. H.; Allara, D. L. *J. Am. Chem. Soc.* **1990**, *112*, 558.
(28) Braun, R. M.; Blenkinsopp, P.; Mullock, S. J.; Corlett, C.; Willey, K. F.; Vickerman, J. C.; Winograd, N. *Rapid Commun. Mass Spectrom.* **1998**, *12*, 1246.
(29) Beamson, G.; Briggs, D.; Davies, S. F.; Fletcher, I. W.; Clark, D. T.; Howard, J.; Gelius, U.; Wannberg, B.; Balzer, P. *Surf. Interface Anal.* **1990**, *15*, 541.
(30) Gelius, U.; Wannberg, B.; Balzer, P.; Fellner-Feldegg, H.; Carlsson, G.; Johansson, C.-G.; Larsson, J.; Munger, P.; Vegerfors, G. *J. Electron Spectrosc. Relat. Phenom.* **1990**, *52*, 747.
(31) Tarlov, M. J.; Newman, J. G. *Langmuir* **1992**, *8*, 1398.
(32) Hutt, D. A.; Cooper, E.; Leggett, G. J. *J. Phys. Chem.* **1998**, *B102*, 174.
(33) Hagenhoff, B.; Benninghoven, A.; Spinke, J.; Liley, M.; Knoll, W. *Langmuir* **1993**, *9*, 1622.
(34) Wood, M. C. Surface Characterization and Imaging with Ion-Induced Desorption and Multiphoton Resonance Ionization. Ph.D. Thesis, The Pennsylvania State University, University Park, PA, 1995; pp 34−111.
(35) Sigmund, P., Ed. *Fundamental Processes in Sputtering of Atoms and Molecules (SPUT92)*; Bianco Lunos Bogtrykkeri: Denmark, 1992; pp 223−254.
(36) Czanderna, A. W., Hercules, D. M., Eds. *Ion Spectroscopies for Surface Analysis*; Plenum Publishing: New York, 1991; pp 45−141.
(37) Mertens, F. P. *Surf. Sci.* **1978**, *71*, 161.
(38) Fisher, G. L.; Hooper, A. E.; Skriba, H. T.; Bahnck, K.; Winograd, N.; Allara, D. L. Manuscript in preparation.
(39) Maslowski, E., Jr. *Vibrational Spectra of Organometallic Compounds*; Wiley & Sons: New York, 1977.
(40) Compton, T. R. *Comprehensive Organometallic Analysis*; Plenum Publishing: New York, 1987; pp 283−308.
(41) Chakraborty, A. K.; Davis, H. T.; Tirrell, M. *J. Polym. Sci.: Polym. Chem.* **1990**, *A28*, 3185.
(42) Chen, J. G.; Basu, P.; Ng, L.; Yates, J. T. *Surf. Sci.* **1988**, *194*, 397.
(43) Rogers, J. W.; White, J. M. *J. Vac. Sci. Technol.* **1979**, *16*, 485.
(44) Rogers, J. W.; Hance, R. L.; White, J. M. *Surf. Sci.* **1980**, *100*, 388.
(45) Basu, P.; Chen, J. G.; Ng, L.; Colaianni, M. L.; Yates, J. T. *J. Chem. Phys.* **1988**, *89*, 2406.
(46) Waddil, G. D.; Kesmodel, L. I. *Surf. Sci.* **1987**, *182*, L248.
(47) Kerkar, M.; Hayden, A. B.; Woodruff, D. P.; Kadadwala, M.; Jones, R. G. *J. Phys.: Condens. Matter* **1992**, *4*, 5043.